Tropical Plants

ARTICLE

Open Access

https://doi.org/10.48130/tp-0026-0019

Tropical Plants **2026**, 5: e018

Genome-wide identification of the laccase phylogenetic family in mango and expression analysis in response to enhanced UV-B radiation treatment

Authors

Yijia Gao, Hassam Tahir, Kaibing Zhou*, Yueming Xiong*

Correspondence

zkb@hainanu.edu.cn (Zhou K);
604078135@qq.com (Xiong Y)

In Brief

A genome-wide analysis identified 54 laccase genes in mango and revealed their evolutionary characteristics, structural conservation, and potential regulatory roles. Expression profiling under enhanced UV-B radiation showed that *MiLAC3* and *MiLAC50* were strongly induced, together with increased ABA and MeJA levels, suggesting their possible involvement in UV-B stress tolerance.

Graphical abstract

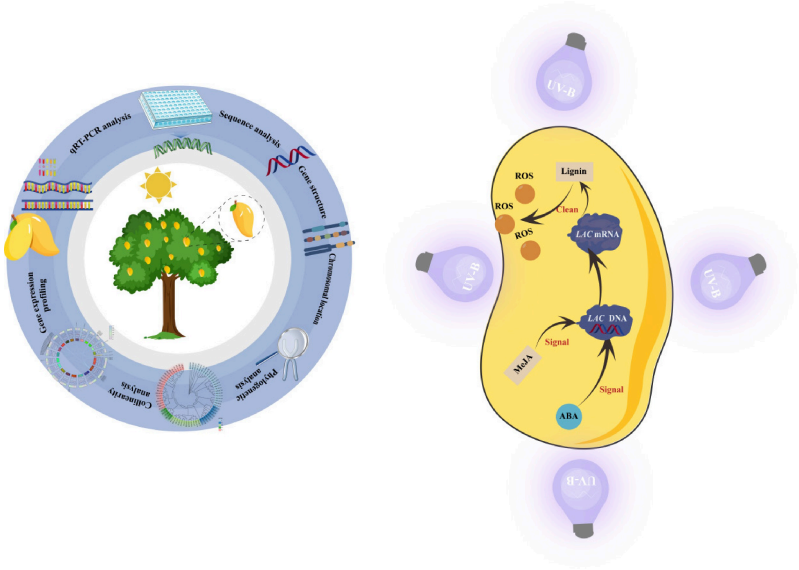

Highlights

- A total of 54 laccase genes (*MiLACs*) were identified in the mango genome.
- The *MiLAC* family was classified into five phylogenetic subgroups with conserved gene structures and protein domains.
- Segmental duplication was the main driver of *MiLAC* family expansion, and most genes underwent purifying selection.
- Promoter analysis revealed abundant light-, hormone-, and stress-responsive *cis*-elements in *MiLAC* genes.
- *MiLAC3* and *MiLAC50* were significantly upregulated under enhanced UV-B radiation and may contribute to mango UV-B stress tolerance.

Citation: Gao Y, Tahir H, Zhou K, Xiong Y. 2026. Genome-wide identification of the laccase phylogenetic family in mango and expression analysis in response to enhanced UV-B radiation treatment. *Tropical Plants* 5: e018 https://doi.org/10.48130/tp-0026-0019

Tropical Plants

ARTICLE

Open Access

https://doi.org/10.48130/tp-0026-0019

Tropical Plants **2026**, 5: e018

Genome-wide identification of the laccase phylogenetic family in mango and expression analysis in response to enhanced UV-B radiation treatment

Yijia Gao[1,2], Hassam Tahir[3], Kaibing Zhou[1,2*] and Yueming Xiong[4*]

[1] *Sanya Institute of Breeding and Multiplication, Hainan University, Sanya 572025, China*
[2] *Key Laboratory of Quality Regulation of Tropical Horticultural Crop in Hainan Province, School of Tropical Agriculture and Forestry, Hainan University, Haikou 570228, China*
[3] *College of Landscape and Horticulture, Yunnan Agriculture University, Kunming 650500, China*
[4] *Institute of Fruit Tree Research, Fujian Academy of Agricultural Sciences , Fuzhou 350013, China*
* Correspondence: zkb@hainanu.edu.cn (Zhou K); 604078135@qq.com (Xiong Y)

Abstract

Laccases are copper-containing polyphenol oxidases involved in plant growth, development, and stress responses. In this study, members of the mango laccase multigene family (*MiLACs*) were identified and characterised, and their expression patterns under enhanced UV-B radiation were analysed to provide a basis for further functional studies. A total of 54 *MiLAC* genes were identified in the mango genome and mapped to 12 chromosomes and one scaffold. The encoded proteins ranged from 237 to 1,147 amino acids, with most being approximately 560 aa in length. Most MiLAC proteins were predicted to be stable and hydrophilic; 43 contained signal peptides, and most were predicted to localise to chloroplasts. Phylogenetic analysis grouped the *MiLAC* family into five subgroups, whose members shared similar gene structures. Segmental duplication appeared to be a major driver of family expansion. In addition, all syntenic gene pairs showed Ka/Ks ratios far below 1, indicating that *MiLACs* have mainly undergone purifying selection during evolution. MiLAC proteins mainly contained conserved blue copper protein domains with three copper oxidase domains. Promoter analysis revealed numerous light-, hormone-, and stress-responsive *cis*-elements, with *MiLAC3* and *MiLAC50* containing the most ABA- and MeJA-responsive elements. Expression analysis showed that *MiLAC3* and *MiLAC50* were significantly upregulated under enhanced UV-B treatment, accompanied by increased ABA and MeJA contents, suggesting that these genes may contribute to UV-B stress tolerance in mango.

Citation: Gao Y, Tahir H, Zhou K, Xiong Y. 2026. Genome-wide identification of the laccase phylogenetic family in mango and expression analysis in response to enhanced UV-B radiation treatment. *Tropical Plants* 5: e018 https://doi.org/10.48130/tp-0026-0019

Introduction

Laccase (LACs, EC 1.10.3.2) is a type of multi-copper oxidase belonging to the blue copper protein superfamily. Its active centre binds four copper ions to form copper oxidase domains[1], enabling it to catalyse the oxidative degradation of various aromatic and non-aromatic compounds (such as phenols, lignin, anilines, thiols, and arylamines)[2]. During catalysis, copper ions absorb and transfer electrons, reducing oxygen to water and generating substrate-derived free radicals that drive the oxidation reaction[3]. Laccases are widely distributed in bacteria, fungi, insects, and plants[4]. They were first discovered by the Japanese scientist Yoshida in the lacquer tree (*Rhus vernicifera*) of the family Anacardiaceae in China[5]. The plant laccase gene family constitutes a medium-sized multigene family[6]. Its primary functions include catalysing lignin biosynthesis, secondary cell wall formation, and the polymerization of phenolic compounds, thereby not only regulating plant growth and development but also playing a key role in enhancing resistance to both biotic and abiotic stresses[7–9].

The plant laccase multigene family (*LACs*) has been identified in numerous species, including *Arabidopsis thaliana*[10], *Citrus sinensis*[11], *Pyrus*[12], *Gossypium*[13], *Populus*[14], and *Oryza sativa*[15], among others. Although the number and types of *LAC* gene family members vary considerably among these different plants, the family is evolutionarily conserved overall, sharing similar domains and conserved active reaction sites, and performing analogous functions. Most plant laccases are involved in the oxidation of monolignols, which contribute to the formation of higher-order lignin structures. In *Arabidopsis thaliana*, which contains 17 *LAC* family members, *AtLAC2*, *AtLAC4*, and *AtLAC17* are believed to participate in lignin biosynthesis, thereby regulating plant growth and development[16–18]. In *Brachypodium distachyon*, the double knockout mutant of *LAC8* and *LAC5* results in a significant decrease in lignin content and a marked increase in saccharification efficiency, without compromising plant integrity[19]. In *Populus deltoides*, a laccase (*PdLAC2*) is associated with the oxidation of phenolic compounds and the binding of flavonoids that interact with lignin[20]. In cotton, the *GhLAC15* gene enhances resistance to Verticillium wilt by increasing cell wall lignin content[21]. In rice (*Oryza sativa*), *OsLAC10* enhances copper (Cu) stress tolerance in *Arabidopsis,* potentially by promoting root lignification to prevent excessive copper uptake, indicating a role in improving plant resistance to heavy metal stress[15]. In sweet orange, cold treatment induces differential regulation of 21 *CsLACs*, accompanied by increased laccase activity and lignin content in leaves; *CsLACs* can be induced by various hormones and abiotic stresses[22]. These findings collectively highlight that plant laccases are not merely structural enzymes, but are dynamic components of the plant's stress response machinery[14,23].

Despite this accumulation of knowledge in other species, the specific biological functions of laccases in mango (*Mangifera indica* L.), an economically important fruit tree of the Anacardiaceae family, remain largely unexplored. This research gap is particularly critical given the current environmental challenges in mango cultivation. Mango is predominantly grown in low-latitude tropical and subtropical regions, where it is frequently exposed to intense environmental stressors, most notably enhanced UV-B radiation (280–315 nm)

resulting from stratospheric ozone depletion. Such elevated UV-B radiation can severely compromise plant cellular integrity, photosynthesis, and ultimately fruit quality and yield[24–26]. Therefore, unravelling the molecular mechanisms underlying mango adaptation to UV-B stress has become an important scientific question.

The theoretical foundation for the involvement of laccases in the UV-B response lies in the protective nature of the secondary metabolites they synthesize. Plant laccases catalyze the polymerization of lignin and phenolic compounds[17], which act as vital physiological screens by accumulating in the epidermal cell walls to absorb deleterious UV radiation[27]. Furthermore, these phenolic products are potent antioxidants capable of scavenging reactive oxygen species (ROS) induced by UV-B exposure, thereby preventing oxidative damage to cellular macromolecules[28,29]. Additionally, plant responses to abiotic stresses, including UV-B radiation, are regulated by endogenous phytohormones, particularly abscisic acid (ABA) and methyl jasmonate (MeJA)[30]. These hormones serve as central signalling molecules that rapidly accumulate under stress conditions and trigger the expression of downstream defense-related genes[31]. However, it remains unclear whether mango laccases participate directly in UV-B stress tolerance, and whether their activity is regulated through ABA- or MeJA-mediated signalling pathways.

To address these scientific questions, a comprehensive genome-wide analysis is necessary to understand how the *MiLAC* gene family responds to environmental radiation. In this study, we utilised genomic data from mango and Arabidopsis to identify *MiLACs*, subsequently analysed their physicochemical properties, phylogeny, chromosomal distribution, and promoter *cis*-acting elements. By integrating transcriptomic data with real-time quantitative polymerase chain reaction (RT-qPCR) validation, we aim to elucidate the expression patterns of *MiLAC* family members under enhanced UV-B radiation.

Materials and methods

Materials

The experimental site is located at the Shengchang Village Mango Orchard, Haitang District, Sanya City, Hainan Province (18°25' N, 109°46' E). The average UV-B radiation intensity in this area is 83.47 kJ·m^{-2}·d^{-1}; the annual average precipitation is about 1,700 mm, and the annual average temperature is about 25 °C. The soil is red sandy loam. The 'Tainong No. 1' mango (*Mangifera indica* L. cv. Tainongyihao) trees are 17 years old and have naturally rounded canopies, planted at a spacing of 4 m × 5 m. The orchard and tree canopies have good ventilation and light penetration. The mango whole-genome sequence and corresponding annotation data were downloaded from the NCBI Datasets resource (www.ncbi.nlm.nih.gov/datasets/taxonomy/29780). The *Arabidopsis thaliana* (L.) Heynh. laccase (AtLAC) gene family sequences were retrieved from the TAIR database (www.arabidopsis.org).

Experimental design

Previous findings from our research group indicated that artificially simulated enhanced UV-B radiation at 96 kJ·m^{-2}·d^{-1}, equivalent to a 15% increase over natural levels, significantly reduced per-plant yield and deteriorated fruit quality in 'Tainongyihao' mango[32]. Therefore, the experimental setup involved installing four 40 W UV-B lamps (λ = 313 nm) uniformly in a cross pattern 40 cm above the canopy to provide enhanced UV-B radiation in the treatment group. The control group received natural sunlight only. The experiment was arranged in a single-tree plot design with five replicates. Field trials were conducted over two consecutive fruit growth cycles: from November 16, 2023 (30 d after flowering) to January 6, 2024 (91 d after flowering), and from March 10, 2024 (30 d after flowering) to May 11, 2024 (92 d after flowering). During each growth cycle, fruit samples were collected at 30, 40, 50, 60, 72, 77, and 91 d after flowering in 2023, and at 30, 40, 51, 61, 71, 81, and 92 d after flowering in 2024 for subsequent physiological and biochemical analyses. The lamps were switched on daily from sunrise to sunset to provide irradiation. The enhanced UV-B treatment was suspended during overcast or rainy weather by turning off the lamps.

Sampling and sample pre-treatment

Five fruits of median size were selected from the middle section on each of the four sides of the canopy periphery of every sample tree as reference fruits for sampling. Fruit samples were collected once at the initiation of the field-enhanced UV-B radiation treatment, and subsequently at 10-d intervals. Sampling was performed according to the size and colour development of the reference fruit. In the field, the peel and pulp were rapidly separated, immediately flash-frozen in liquid nitrogen, transported back to the laboratory, and stored in a −80 °C ultra-low temperature freezer for subsequent use.

Identification of the LAC gene family in mango

Using the protein sequences of the *AtLAC* gene family members as a reference, a local BLAST analysis was performed against the mango protein database using TBtools software, yielding 54 protein sequences as candidate mango laccases (*MiLACs*). Hidden Markov models (HMMs) for the Cu-oxidase domain families (Cu-oxidase: PF00394, Cu-oxidase-2: PF07731, and Cu-oxidase-3: PF07732) were downloaded from InterPro (www.ebi.ac.uk/interpro)[33] and used as queries to search the protein dataset using HMMER 3.0. Candidate genes were initially identified using the NCBI online CD-search tool (www.ncbi.nlm.nih.gov/Structure/cdd/wrpsb.cgi). To ensure accurate identification, the candidate *MiLAC* genes were further validated using the SMART database (http://smart.embl-heidelberg.de), and redundant sequences as well as proteins lacking the conserved domains were removed, yielding the final set of *MiLAC* gene family members.

Protein characterisation of LAC genes

The physicochemical properties of MiLAC proteins—including amino acid length, molecular weight (MW), and theoretical isoelectric point (pI)—were predicted using the online tool ProtParam (http://web.expasy.org/protparam). Subcellular localization was predicted with WoLF PSORT (https://wolfpsort.hgc.jp). Signal peptides were predicted using the SignalP 5.0 online server (https://services.healthtech.dtu.dk/service.php?SignalP-5.0).

Gene structures and conserved motifs analysis

The filtered MiLAC protein sequences were submitted to the NCBI Batch Web CD-Search tool (www.ncbi.nlm.nih.gov/Structure/bwrpsb/bwrpsb.cgi) to identify conserved domains. The corresponding protein sequences were then analysed using MEME (https://meme-suite.org/meme/tools/meme) to detect conserved motifs, with the maximum number of motifs set to 10. All results were visualised using TBtools.

Phylogenetic relationship of the LAC gene family in mango

A multiple sequence alignment was used to determine the evolutionary relationship among mango *LAC* genes and their homologs in *A. thaliana* using the MUSCLE algorithm, based on a total of 71 protein sequences (54 from *Mangifera indica* and 17 from *Arabidopsis thaliana*). Phylogenetic analysis was performed in MEGA 11 using the Maximum Likelihood (ML) method based on the identified protein sequences from different species, with bootstrap resampling set to 1,000 replicates to assess node support. The resulting phylogenetic tree was subsequently visualised using the online tool Chiplot (https://chiplot.online).

Chromosomal mapping and Ka/Ks ratio evaluation

Intraspecies synteny analysis in mango was conducted using TBtools. Based on whole-genome annotation files, gene density across the genome and the chromosomal distribution of *MiLAC* genes were determined. Using the genome assembly (whole-genome sequence) file, chromosomal GC content and gap regions were calculated. The Ka and Ks substitution rates of homologous gene pairs were estimated using the natural gradient descent (NG) method, and the resulting Ka/Ks ratios were used to assess selective pressure.

Identification of *cis*-elements in the promoter region of LAC genes

Based on the mango gene family sequence information, the 2,000-bp upstream promoter regions of *MiLACs* genes were extracted using TBtools. These promoter sequences were then submitted to PlantCARE (http://bioinformatics.psb.ugent.be/webtools/plantcare/html) for *cis*-acting regulatory element prediction, and the results were visualised with TBtools.

Screening of differentially expressed genes and qPCR validation

Based on previously published transcriptome data from our group[34] (the mango transcriptome dataset is available in the NCBI database under accession number PRJNA1245353), two highly expressed *MiLAC* genes were selected as key targets for investigation during 2023–2024 (Table 1). Gene-specific qPCR primers were designed using the NCBI Primer-BLAST online tool (www.ncbi.nlm.nih.gov/tools/primer-blast; accessed December 1, 2024), and primer synthesis was performed by Shanghai Shengxin Biotechnology Co., Ltd. (Shanghai, China).

Total RNA was extracted from mango pulp using the SteadyPure Plant RNA Extraction Kit (Cat. No. AG21024; Hunan Accurate Biotechnology Co., Ltd., Changsha, China). First-strand cDNA synthesis was carried out using the Evo M-MLV Reverse Transcription Premix Kit (Cat. No. AG11728; Hunan Accurate Biotechnology Co., Ltd.) on a BIO-RAD T100™ thermal cycler, following the manufacturer's instructions. Quantitative PCR was performed using the SYBR® Green Premix Pro Taq HS qPCR Kit (Cat. No. AG11701; Hunan Accurate Biotechnology Co., Ltd.) on a qTOWER3 real-time PCR system (Analytik Jena AG, Jena, Germany). The thermal cycling protocol was as follows: 95 °C for 10 min, followed by 40 cycles of 95 °C for 5 s, 60 °C for 30 s, and 72 °C for 30 s. All experiments were performed with three biological replicates and three technical replicates. The mango Actin gene was used as the internal reference, and relative transcript levels were calculated using the $2^{-\Delta\Delta C_T}$ method. Primer sequences are listed in Supplementary Table S1.

Detection method of hormone levels in mango flesh

The contents of abscisic acid (ABA) and methyl jasmonate (MeJA) were determined using Enzyme-Linked Immunosorbent Assay (ELISA) kits (Catalog No: YJ077235, YJ077224; Shanghai Enzyme-linked Biotechnology Co., Ltd.) according to the manufacturer's instructions. A standard curve was generated using the standard solutions provided in the kit (R2 > 0.9900). After colour development, the optical density (OD) was measured at a wavelength of 450 nm using a microplate reader (Multiskan FC, Thermo Fisher). The concentrations of ABA and MeJA in the samples were calculated based on the standard curve and expressed as ng/g fresh weight (FW) and pmol/g.

Data processing and statistical analysis

Statistical analysis was performed using SAS software. A Student's *t*-test was used to assess the significance of differences between treatment and control groups ($p < 0.05$ was considered statistically significant, and $p < 0.01$ was considered highly significant). ANOVA was used to analyse variance in dynamic changes, and Duncan's method was used for multiple comparisons at different time points.

Results

MiLACs identification and phylogenetic analysis

A total of 54 *MiLAC* genes were identified in the mango genome, and they were named *MiLAC1* to *MiLAC54* based on the naming convention used for Arabidopsis genes. In this study, the protein lengths, molecular weights, isoelectric points, instability indices, fat coefficients, hydrophilicity, signal peptides, and subcellular localisation information of the 54 members of the mango laccase gene family were summarised, as shown in Table 1.

The protein lengths of the mango laccase gene family members range from 237 to 1,147 amino acids, with most proteins approximately 560 amino acids in length. The longest protein is *MiLAC53*, and the shortest is *MiLAC3*. There is a certain degree of variation in protein length among the different members, which may be related to the functional diversity of the members. As shown in Table 1, the molecular weights of the MiLAC proteins range from 25,893.89 to 126,257.25 Da, with theoretical isoelectric points ranging from 4.58 to 10.07. The instability indices of the proteins range from 24.53 to 40.64. Except for *MiLAC33*, all other *MiLAC* proteins have instability indices below 40, indicating that the proteins in this gene family generally have stable structures. The fat coefficients range from 76.02 to 90.09, and the hydrophilicity values range from −0.275 to 0.014. Except for *MiLAC4*, whose protein is hydrophobic, all other 53 *MiLAC* proteins are hydrophilic. Moreover, out of the 54 *MiLAC* genes, 43 contain signal peptides, while 11 genes (*MiLAC3*, *MiLAC12*, *MiLAC30*, *MiLAC34*, *MiLAC42*, *MiLAC43*, *MiLAC46*, *MiLAC48*, *MiLAC52*, *MiLAC53*, and *MiLAC54*) do not. This suggests that most members of this gene family are secretory proteins lacking transmembrane domains. Subcellular localization analysis (Table 1) revealed that the 54 *MiLACs* are unevenly distributed across various cellular locations, including the extracellular space, cytoplasm, nucleus, plasma membrane, endoplasmic reticulum, chloroplast, peroxisome, and cytoskeleton. Among them, 26 are localised to the chloroplasts, 12 to the vacuole, seven to the extracellular space, five to the cytoplasm, three to the nucleus, two to the peroxisome, two to the plasma membrane, and one each in the cytoskeleton and endoplasmic reticulum.

Table 1. Basic information on *MiLAC* proteins.

Gene ID	Gene name	Number of amino acid	Molecular weight	pI	Instability index	Aliphatic index	Grand average of hydropathicity	Signal peptide	Subcellular localization
LOC123201611.1	*MiLAC1*	556	60,749.63	9.08	35.24	88.29	−0.041	YES	chlo
LOC123205456.1	*MiLAC2*	584	64,386.08	9.52	29.79	83.75	−0.076	YES	chlo
LOC123229717.1	*MiLAC3*	1147	126,257.25	5.19	34.44	80.51	−0.092	NO	plas
LOC123224994.1	*MiLAC4*	572	63,281.91	9.1	27.84	89.3	0.014	YES	chlo
LOC123209589.1	*MiLAC5*	578	64,417.75	8.48	36	78.58	−0.149	YES	extr
LOC123192083.1	*MiLAC6*	572	63,621.29	10.07	27.3	86.89	−0.091	YES	chlo
LOC123209528.1	*MiLAC7*	553	61,191.25	8.47	36.03	89.51	−0.056	YES	vacu
LOC123216306.1	*MiLAC8*	572	63,469.53	6.37	39.47	84.84	−0.043	YES	chlo
LOC123228608.1	*MiLAC9*	566	63,672.79	6.67	31.23	83.14	−0.127	YES	plas
LOC123229715.1	*MiLAC10*	574	64,038.58	6.59	33.01	76.74	−0.194	YES	pero
LOC123229713.1	*MiLAC11*	567	63,081.24	5.7	31.88	79.58	−0.146	YES	vacu
LOC123229041.1	*MiLAC12*	489	54,460.42	5.51	32.9	79.71	−0.18	NO	cyto
LOC123192537.1	*MiLAC13*	555	60,981.79	9.05	25.26	88.52	−0.045	YES	extr
LOC123198235.1	*MiLAC14*	568	63,437.73	6.37	34.2	77.2	−0.171	YES	vacu
LOC123229003.1	*MiLAC15*	561	62,323.26	6.07	33.51	82.51	−0.098	YES	vacu
LOC123201553.1	*MiLAC16*	557	60,936.06	9.09	33.74	90.09	−0.023	YES	chlo
LOC123228569.1	*MiLAC17*	582	65,830.37	5.57	38.25	78.83	−0.237	YES	nucl
LOC123206493.1	*MiLAC18*	568	63,338.6	6.37	35.12	77.2	−0.183	YES	vacu
LOC123229720.1	*MiLAC19*	568	63,373.65	6.54	33.88	76.51	−0.18	YES	vacu
LOC123203686.1	*MiLAC20*	561	62,591.07	6.43	35.67	76.45	−0.15	YES	pero
LOC123201619.1	*MiLAC21*	555	60,688.79	9.33	35.32	88.13	−0.055	YES	chlo
LOC123204379.1	*MiLAC22*	582	64,553.83	9.01	33.26	78.61	−0.161	YES	chlo
LOC123229716.1	*MiLAC23*	570	63,427.87	6.75	33.8	79.33	−0.175	YES	chlo
LOC123229257.1	*MiLAC24*	563	63,486.69	8.41	34.99	82.4	−0.168	YES	chlo
LOC123229178.1	*MiLAC25*	568	63,154.61	6.53	33.09	77.04	−0.177	YES	chlo
LOC123229004.1	*MiLAC26*	560	62,105.23	6.2	33.31	82.84	−0.088	YES	vacu
LOC123228609.1	*MiLAC27*	561	62,326.46	6.02	34.23	83.39	−0.077	YES	vacu
LOC123206108.1	*MiLAC28*	572	63,240.64	8.74	31.83	87.9	−0.034	YES	chlo
LOC123201844.1	*MiLAC29*	578	63,603.97	9.14	28.91	83.49	−0.063	YES	chlo
LOC123229714.1	*MiLAC30*	549	60,833.73	6.05	35.5	77.58	−0.215	NO	cyto
LOC123227135.1	*MiLAC31*	574	63,105.94	7.63	31.52	81.86	−0.051	YES	chlo
LOC123229712.1	*MiLAC32*	561	62,131.03	5.69	34.2	83.58	−0.074	YES	vacu
LOC123229362.1	*MiLAC33*	582	65,859.48	5.35	40.64	83.38	−0.204	YES	nucl
LOC123229040.1	*MiLAC34*	568	63,650.32	8.78	35.14	76.02	−0.275	NO	vacu
LOC123192675.1	*MiLAC35*	574	63,699.53	6.4	31.04	76.92	−0.073	YES	chlo
LOC123230046.1	*MiLAC36*	580	65,597.04	5.53	37.77	78.97	−0.261	YES	extr
LOC123198865.1	*MiLAC37*	561	62,316.52	7.69	35.58	84.3	−0.121	YES	chlo
LOC123201999.1	*MiLAC38*	566	62,256.27	8.69	30.64	85.92	−0.021	YES	vacu
LOC123229061.1	*MiLAC39*	564	62,158.85	4.83	35.2	78.67	−0.105	YES	extr
LOC123228568.1	*MiLAC40*	582	65,548.8	5.33	38.46	79.54	−0.267	YES	nucl
LOC123229436.1	*MiLAC41*	578	63,779.86	9.04	29.33	80.93	−0.097	YES	chlo
LOC123216462.1	*MiLAC42*	499	55,377.93	6.45	36.53	79.66	−0.117	NO	cyto
LOC123229209.1	*MiLAC43*	569	62,757.79	5.44	35.49	78.51	−0.093	NO	extr
LOC123206286.1	*MiLAC44*	552	61,357.32	7.66	36.69	86.5	−0.106	YES	vacu
LOC123229039.1	*MiLAC45*	569	63,648.25	6.1	35.15	79.02	−0.189	YES	chlo
LOC123229164.1	*MiLAC46*	569	62,698.66	5.52	35.51	79.02	−0.099	NO	extr
LOC123209471.1	*MiLAC47*	557	61,890.37	8.69	29.79	89.89	−0.036	YES	chlo
LOC123202218.1	*MiLAC48*	464	51,228.21	9.68	24.53	79.44	−0.176	NO	cyto
LOC123230053.1	*MiLAC49*	569	63,418	6.17	32.88	76.1	−0.202	YES	E.R.
LOC123229109.1	*MiLAC50*	569	63,430.15	6.62	32.22	76.1	−0.193	YES	chlo
LOC123216139.1	*MiLAC51*	566	62,425.18	8.43	32.58	83.22	−0.071	YES	chlo
LOC123208638.1	*MiLAC52*	589	65,038.69	8.96	32.73	87.57	−0.038	NO	extr
LOC123229718.1	*MiLAC53*	237	25,893.89	4.58	26.69	77.76	−0.093	NO	cyto
LOC123230055.1	*MiLAC54*	406	44,523.01	5.25	37.31	76.4	−0.138	NO	cysk

chlo: chloroplast; plas: plasma membrane; extr: extracellular; vacu: vacuole; cyto: cytoplasm; nucl: nucleus; pero: peroxisomes; E.R.: endoplasmic reticulum; cysk: cytoskeleton.

Phylogenetic tree construction of the *MiLAC* gene family

To investigate the phylogenetic relationships and classification of the *MiLAC* family members, a phylogenetic tree was constructed using the amino acid sequences of 54 *MiLACs* and 17 *AtLACs* family members, based on protein homology (Fig. 1). The results revealed that the *MiLAC* and *AtLAC* genes were divided into five subfamilies. Among them, *AtLACs* were distributed across subfamilies II, III, IV, and V, while *MiLACs* were primarily distributed in subfamily I, with 23 members; 16 members were located in subfamily V, seven in subfamily II, five in subfamily III, and three in subfamily IV. *LACs* within the same subfamily are likely to share similar biological functions.

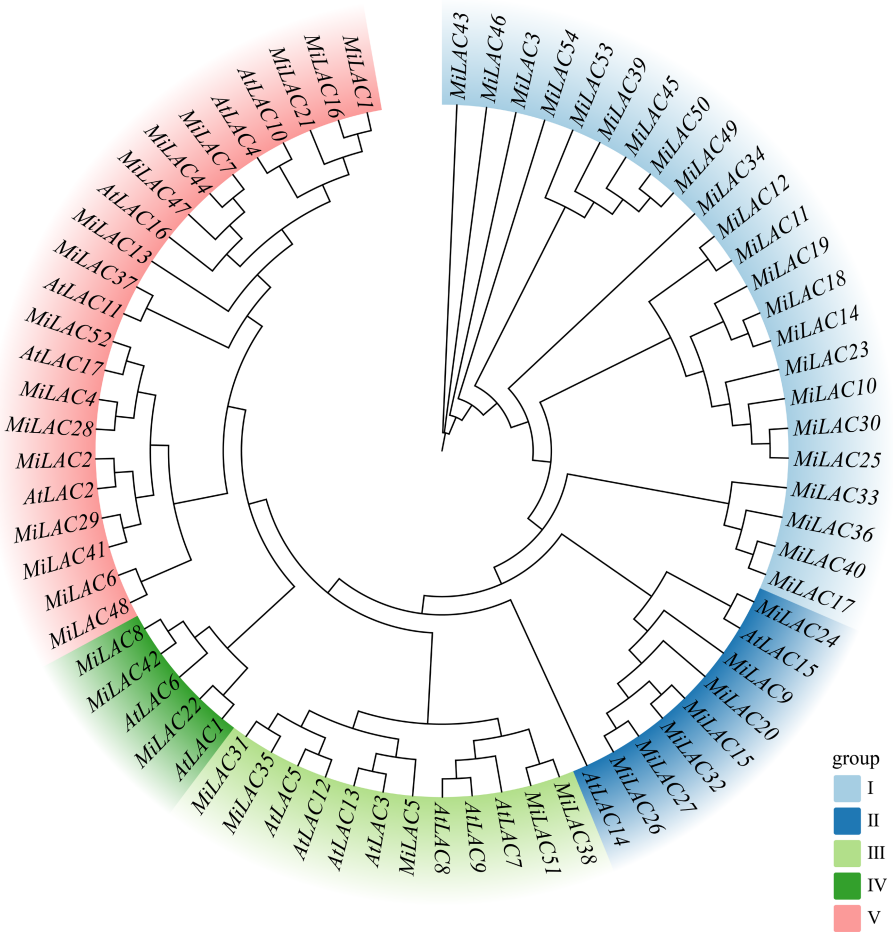

Fig. 1 Phylogenetic tree of *MiLACs*.

Analysis of conserved domains in *MiLACs* structural proteins

Using the MEME online tool, 10 conserved motifs were identified in the protein sequences of all *MiLAC* family members, and the conserved sequences of these motifs were summarised (Supplementary Table S2). Additionally, the structure of the 54 *MiLACs* genes was analysed using TBtools software (Fig. 2). Among the 54 *MiLACs*, Motif 1, Motif 7, and Motif 2 were present in 52 *MiLACs*, Motif 3, Motif 5, and Motif 10 were found in 53 *MiLACs*, and Motif 4 was present in 50 *MiLACs*. Meanwhile, Motif 9, Motif 8, and Motif 6 were conserved across in all 54 protein sequences. The length of each conserved motif ranged from 15 to 50 amino acids, indicating a high degree of conservation in the protein domains of this gene family. The conserved motifs were further verified using the Pfam database, which revealed that three motifs correspond to three distinct copper oxidase domains (Cu_oxidase, Cu_oxidase_2, and Cu_oxidase_3). Specifically, Motif 1 fully corresponds to the Cu_oxidase_3 domain, Motif 2 matches the Cu_oxidase domain, and Motif 3 constitutes the Cu_oxidase_2 domain. The number of introns in the *MiLACs* genes ranged from two to 14, with 25 genes containing five introns. The coding regions of *MiLAC3*, *MiLAC47*, *MiLAC7*, and *MiLAC44* exhibited higher variability, with these regions separated by relatively long introns. Variations in the number and distribution of exons and introns across different *MiLAC* genes may be associated with the functional differentiation of these genes.

MiLACs chromosomal localization, synteny analysis, and selective pressure analysis

In this study, the chromosomal localization map of the *MiLAC* genes and the syntenic relationships between the members were plotted based on their positional information (Fig. 3). The *MiLAC* genes are distributed across 12 chromosomes and one scaffold fragment. No *MiLAC* genes were located on chromosomes 3, 4, 6, 7, 8, 13, 14, or 17. The overall distribution of the gene family on the chromosomes is dispersed, but some members are more closely clustered. The highest concentration of *MiLACs* was found on chromosome 11, with 27 genes, followed by chromosome 2 with seven genes, chromosome 18 with six, chromosome 1 with three, and chromosome 5 with two genes, and on chromosome 5, two *MiLACs* were clustered. The remaining chromosomes each contained a single *MiLAC* gene.

Synteny analysis within the mango genome revealed 45 *MiLAC* genes (83%) involved in tandem duplication and were distributed across 5 chromosomes: Chr1, Chr2, Chr5, Chr11, and Chr18. A total of 10 pairs of homologous relationships were identified among 16 *MiLACs*, distributed across nine chromosomes and one scaffold fragment. Furthermore, most members exhibit multiple syntenic relationships with different members, suggesting that segmental duplication is the main driving force behind the evolutionary expansion of the *MiLAC* gene family. These pairs of syntenic genes have likely undergone whole-genome duplication events or have extremely similar gene functions and roles. As shown in Table 2, the Ka/Ks ratios between homologous gene pairs are all well below one,

Fig. 2 Gene structure and motif analysis of *MiLAC*.

indicating that the *MiLAC* genes have mainly undergone purifying selection pressure during their evolutionary process.

Cis-acting element analysis of *MiLAC* promoter regions

The 2,000 bp upstream regions of the 54 *MiLAC* genes were analysed to identify potential regulatory motifs. After removing uncharacterized sequences, the identified elements were classified into three major categories: abiotic stress-related elements, plant hormone signalling-related elements, and growth and development-related elements (Fig. 4).

In the stress-related group, five elements were found, corresponding to light response, antioxidant defence, anaerobic conditions, stress and adversity response, and drought and low-temperature response. The results indicate that each MiLAC promoter region contains varying numbers of light-responsive elements, including TCCC-motif, TCT-motif, GATA-motif, GA-motif, AE-box, chsCMA1a, GT1-motif, I-box, Box 4, G-Box, AAAC-motif, 4cl-CMA2b, L-box, MRE, ATCT-motif, Box II, chsCMA2a, 3-AF1 binding site, CAG-motif, AT1-motif, ACA-motif, ACE, ATC-motif, chs-Unit 1 m1, Gap-box, GTGGC-motif, LAMP-element, TCCC-motif, TCT-motif, and Sp1.

Fig. 3 Chromosome distribution and collinearity analysis of the *MiLACs*.

Table 2. Ka and Ks analysis of *MiLACs* replication gene pairs.

Seq_1	Seq_2	Ka	Ks	Ka/Ks
MiLAC6	*MiLAC2*	0.205375182	1.971231992	0.104186206
MiLAC2	*MiLAC29*	0.186898577	2.325797136	0.080358933
MiLAC28	*MiLAC4*	0.050855744	0.360717481	0.140984973
MiLAC6	*MiLAC5*	0.423715485	–	–
MiLAC5	*MiLAC35*	0.216972756	1.462202414	0.148387633
MiLAC7	*MiLAC13*	0.265466731	1.557947571	0.170395163
MiLAC14	*MiLAC18*	0.002294457	0.017957249	0.127773291
MiLAC27	*MiLAC20*	0.133210788	0.511023074	0.260674703
MiLAC31	*MiLAC35*	0.058176459	0.272809991	0.213249005
MiLAC51	*MiLAC38*	0.080871157	0.579130917	0.139642272

'–': the differences between sequences are too large, resulting in low similarity.

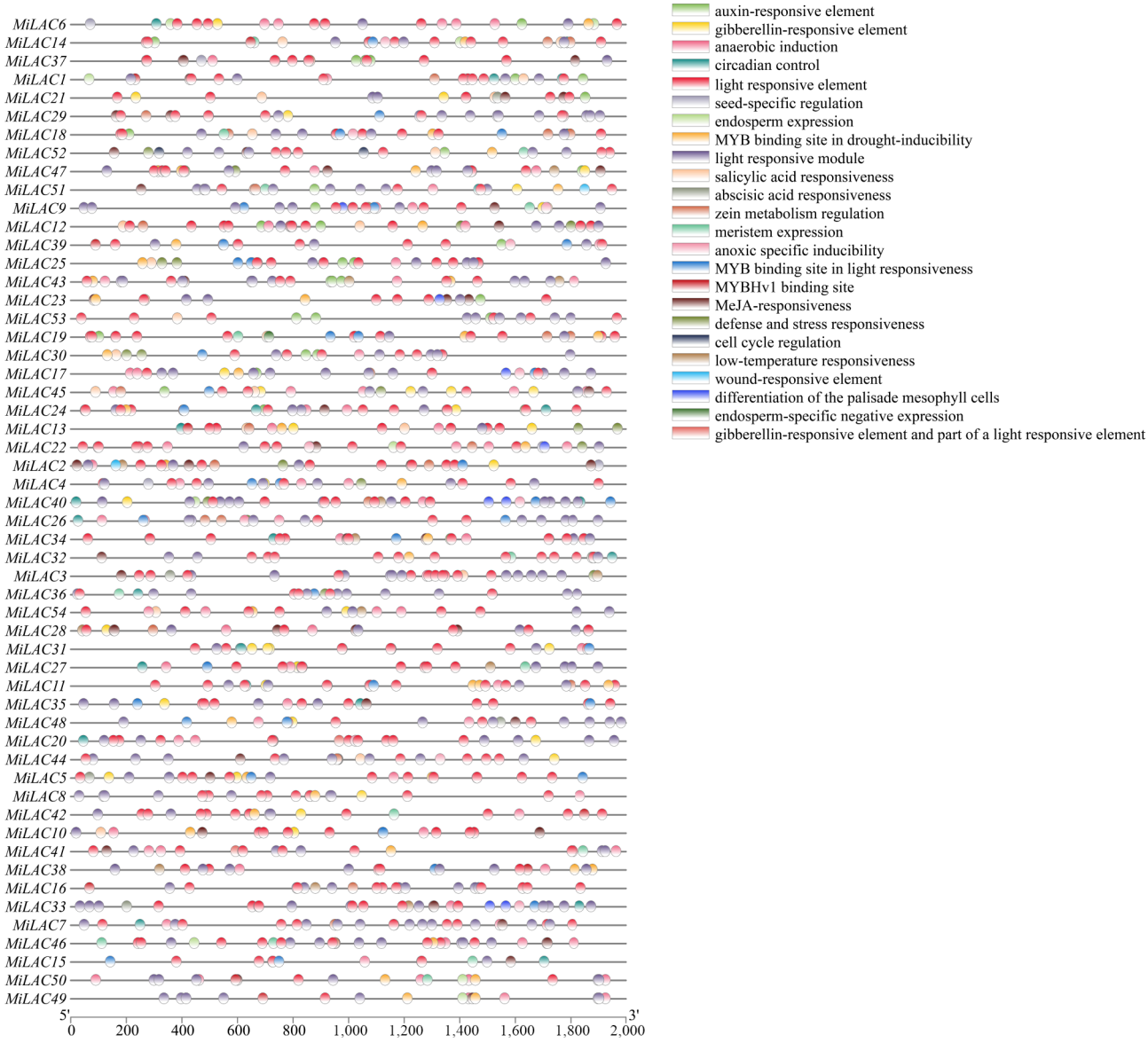

Fig. 4 Analysis of *cis*-acting elements of *MiLACs* promoter.

Particularly noteworthy is the G-box element, a core regulatory motif involved in both light signalling and hormonal pathways, which was detected in all 54 *MiLAC* promoters. The widespread presence of these light-responsive elements suggests that MiLAC expression may be subject to intricate regulation by light signals, thereby contributing to plant adaptation to varying light conditions and stress responses. Additionally, antioxidant response elements (AREs), known to play a key role in reactive oxygen species scavenging and the maintenance of redox homeostasis, were identified in the promoter regions of 42 *MiLACs*. This is especially relevant given that enhanced UV-B radiation is known to trigger a surge in intracellular reactive oxygen species. The convergence of both light-responsive and antioxidant regulatory motifs within the *MiLAC* promoters points to a possible dual role for these genes in mediating UV-B stress tolerance. Anaerobic-induced enhancer-like elements (GC-motif) were present in 10 *MiLAC* promoter sequences, defence and stress response elements (TC-rich repeats) were identified in 19 *MiLAC* promoters, drought stress response elements (MBS) were observed in 33 *MiLAC* promoters, and cold stress response elements (LTR) were detected in 14 *MiLAC* promoters. Regarding plant hormones, five types of hormone-related elements were identified: abscisic acid (ABA) response elements (ABRE) were present in 39 *MiLAC* promoters; auxin response elements (TGA) were found in 22 *MiLAC* promoters; gibberellin response elements (GARE-motif, P-box, TATC-box) were present in 27 *MiLAC* promoters; methyl jasmonate (MeJA) response elements (CGTCA-motif, TGACG-motif) were identified in 30 *MiLAC* promoters; and salicylic acid (SA) response elements (TCA-element, SARE) were present in eight *MiLAC* promoters. Notably, the most common elements were the ABRE (ABA) and CGTCA-motifs, and the TGACG-motif (MeJA), with *MiLAC3* and *MiLAC50* containing the highest number of *cis*-acting elements, which are primarily ABA and MeJA response elements. This highlights the significant role of the *MiLAC* family in hormone regulation.

Additionally, six growth and development-related elements were identified, including meristem-specific expression elements (CAT-box) in 14 *MiLAC* promoters; circadian rhythm regulation elements (circadian) in 20 *MiLAC* promoters; seed-specific elements (RY element) in five *MiLAC* promoters; zein metabolism elements (O2-site) in 21 *MiLAC* promoters; MYBHv1 binding sites (CCAAT-box) in

nine *MiLAC* promoters; and endosperm-specific expression elements (GCN4) in eight *MiLAC* promoters. The dominance of the O2-site element suggests that *MiLACs* may be involved in developmental processes. Cis-acting element analysis revealed that the *MiLAC* family is extensively involved in light morphogenesis, antioxidant responses, hormone signalling, and other growth and development mechanisms. The richness and diversity of these elements suggest that *MiLACs* play a crucial role in mango's adaptation to environmental stimuli and developmental regulation.

Expression analysis of MiLACs under UV-B stress and qRT-PCR validation

To investigate the impact of enhanced UV-B treatment on mango pulp, the expression levels of *MiLAC* genes associated with the lignin biosynthesis pathway were analysed and compared with the control group. Based on transcriptome data and the lignin synthesis pathway (phenylpropanoid biosynthesis, ko00940), a differential gene expression heatmap was generated (Supplementary Fig. S1). In both 2023 and 2024, *MiLAC3* and *MiLAC50* were selected as representative family members for quantitative real-time PCR (qRT-PCR) validation over two consecutive years. The results (Fig. 5) showed that, at 50 d post-flowering in 2023 and 61 d post-flowering in 2024, the expression levels of MiLAC3 and MiLAC50 were significantly higher in the treated group compared to the control group, which is consistent with the transcriptome analysis. These results indicate that enhanced UV-B radiation treatment increases the expression of key *MiLAC* genes, thereby enhancing LAC activity and subsequently promoting lignin accumulation in the mango pulp. This process may help mitigate oxidative damage to the pulp, providing a protective effect against reactive oxygen species.

Effects of enhanced UV-B radiation treatment on ABA and MeJA levels in mango pulp

The dynamic changes in hormone levels between the treatment and control groups in mango pulp were consistent both within and between years, with significant differences observed at different sampling time points. Over the 2 years, the trends in hormone levels at the same sampling time point were generally similar between the treatment and control groups (Fig. 6).

ABA content tended to be higher in the treatment group overall, with significant differences observed at 51 and 61 d after flowering. However, at 40 and 81 d after flowering in 2024, ABA levels were significantly lower in the treatment group compared to the control. MeJA content was higher in the treatment group during the mid-stage of rapid fruit expansion. The main interannual variation was observed at 40 d after flowering in 2024; MeJA content was significantly lower in the treatment group, while no significant difference was observed at the same period in 2023. For both hormones, no significant differences were found between the treatment and control groups at the remaining sampling time points. In summary, despite subtle year-to-year fluctuations in hormone levels between the treatment and control groups, the overall trends over the 2 years were consistent. Together with the finding that *MiLAC3* and *MiLAC50* promoters contain the most ABA and MeJA response elements and exhibit upregulated expression, this suggests that enhanced UV-B radiation treatment may upregulate

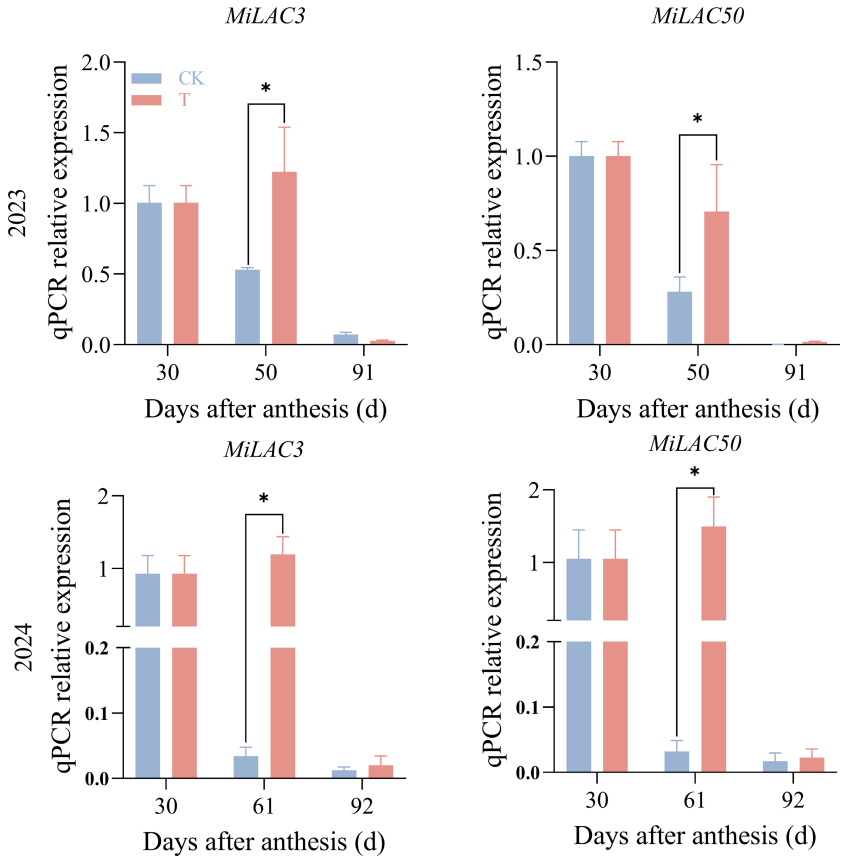

Fig. 5 q-PCR results of *MiLACs* under enhanced UV-B radiation treatment. Note: the two images in the first row are from 2023, and the two images in the second row are from 2024.

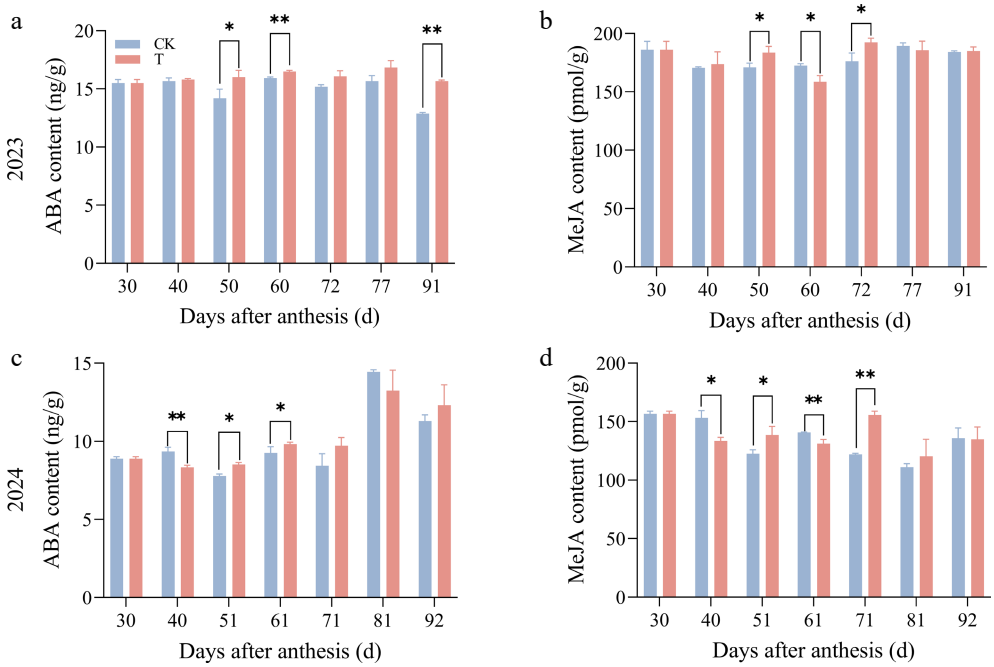

Fig. 6 Effect of enhanced UV-B radiation treatment on ABA and MeJA content changes in the pulp of 'Tainongyihao' mango.

MiLAC3 and *MiLAC50* expression by increasing ABA and MeJA levels in mango pulp.

Discussion

In this study, a total of 54 *MiLACs* were identified. Comparative analysis with species such as *Arabidopsis thaliana*, strawberry, sugarcane, potato, *Populus davidiana* × *P. bolleana*, sweet orange, canola, cotton, sorghum, and *Eucalyptus grandis* revealed variations in the number of gene family members. These differences may be attributed to variations in genome size and gene duplication events during the evolutionary processes of these species[35]. The *MiLAC* gene family was classified into five subfamilies, a clustering pattern consistent with findings in species such as strawberry[36] and potato[37]. Notably, Subfamily I contained the largest number of *MiLAC* members, whereas *Arabidopsis thaliana LACs* were entirely absent from this subgroup. This stark contrast strongly suggests that Subfamily I represents a mango-specific expansion branch. Such an expansion reflects distinct duplication events and subsequent functional divergence experienced by mango during its evolution. Gene duplication serves as the primary driver of gene family expansion. Our analysis indicates that both tandem and segmental duplications have played pivotal roles in the evolution of *MiLACs*, not only facilitating the genesis of novel genes but also driving functional diversification[38]. The uneven distribution of *MiLACs* across different chromosomes may be attributed to tandem or whole-genome duplication events; furthermore, such a distribution pattern may be intrinsically linked to specific biological functions during mango fruit growth and development. Despite these genetic variations, *MiLACs* exhibit a high degree of evolutionary conservation. Members within the same subfamily share similar exon-intron structures and conserved motifs, implying that they likely possess analogous biological functions.

Analysis of *cis*-acting elements in the promoter regions further corroborates this conservation and provides crucial clues regarding their regulatory networks. Similar to *LACs* in peach[39], apple[40], and amaranth[41], the promoter regions of *MiLACs* are enriched with light-responsive elements, highlighting the genetic conservation of *LACs* across different plant species in response to light signaling. Furthermore, the *MiLACs* promoters contain a diverse array of hormone and stress-responsive elements. Elements responsive to phytohormones such as abscisic acid (ABA), methyl jasmonate (MeJA), and salicylic acid (SA) are particularly prevalent. These hormones frequently act as pivotal secondary messengers that bridge the perception of abiotic stress to the activation of downstream defense genes[42]. Consistent with research on potato *LACs*[37], the presence of these elements in *MiLACs* promoters suggests they may be induced under various stress conditions, thereby participating in the regulation of antioxidant functions. Among them, the promoters of *MiLAC3* and *MiLAC50* displayed the greatest abundance of cis-elements, being enriched with ABA-responsive and MeJA-responsive elements, respectively.

Importantly, the temporal dynamics of ABA and MeJA contents (Fig. 6) closely paralleled the expression patterns of *MiLAC3* and *MiLAC50*, with both hormones and transcripts peaking during the middle to late fruit development stages. This correlation, observed across both years despite interannual absolute differences, supports the idea that endogenous ABA and MeJA functionally induce *MiLAC3* and *MiLAC50* expression in a concentration-dependent manner, linking hormone accumulation to laccase-mediated lignin biosynthesis.

To synthesize these molecular findings with physiological adaptations, we propose a coherent regulatory network linking UV-B radiation, hormone signaling, and lignin biosynthesis. Previous research by our group demonstrated that enhanced UV-B radiation treatment significantly improves the resistance of mango fruit to environmental stress. The underlying mechanism begins with the perception of UV-B, which rapidly promotes the accumulation of endogenous phytohormones, notably ABA, SA, and MeJA, in the pulp during the mid-stage of rapid fruit expansion[26]. These stress-responsive hormones then act as signaling molecules that specifically bind to the corresponding enriched cis-acting elements within the promoters of specific laccase genes. This binding event directly

triggers the transcriptional upregulation of these genes, which aligns perfectly with our observation that the promoters of *MiLAC3* and *MiLAC50* are exceptionally rich in ABA and MeJA response elements.

Following this hormone-mediated gene expression, the increased abundance of MiLAC enzymes catalyzes the polymerization of phenolic precursors, driving the synthesis of lignin. Indeed, our earlier work indicated that the lignin content in fruit treated with enhanced UV-B radiation was significantly higher than in the control group. Lignin accumulation aids in dissipating the stress effects caused by UV-B radiation by acting as a physical screen and mitigates cellular damage by scavenging reactive oxygen species, thus enhancing the fruit's overall adaptability to adversity[26]. Consequently, these results support that enhanced UV-B radiation induces ABA and MeJA accumulation, which in turn activates the expression of *MiLAC3* and *MiLAC50* via promoter binding. The upregulated laccases then promote lignin accumulation during mango fruit maturation, ultimately strengthening the fruit's structural and biochemical tolerance to UV-B stress.

Conclusions

The mango *LAC* gene family consists of 54 members, exhibiting both conservation and evolutionary divergence. Segmental duplication appears to be a major evolutionary mechanism driving the expansion of this gene family. Most members contain hormone and stress response elements, suggesting that they play regulatory roles in response to stress and hormonal signalling. Under enhanced UV-B radiation treatment, mango fruit likely upregulates the expression of *MiLAC3* and *MiLAC50* by increasing the levels of ABA and MeJA, which in turn promotes lignin synthesis, enhances resistance to reactive oxygen species (ROS) damage, and alleviates the harmful effects of UV-B radiation stress, thereby improving resistance to enhanced UV-B stress. These findings provide a theoretical foundation for future functional studies of *MiLACs* and offer valuable insights for developing breeding strategies and cultivation techniques to enhance mango's resistance to enhanced UV-B radiation stress.

Author contributions

The authors confirm their contributions to the paper as follows: study conception and design: Gao Y, Zhou K, Xiong Y; data collection: Gao Y, Tahir H; analysis and interpretation of results: Gao Y, Tahir H, Xiong Y, Zhou K; draft manuscript preparation: Gao Y; supervision, project administration, funding acquisition: Zhou K. All authors reviewed the results and approved the final version of the manuscript.

Data availability

The data that support the findings of this study are available from the corresponding author upon reasonable request.

Acknowledgments

This work was financially supported by the National Natural Science Foundation of China (No. 32160677), the Natural Science Foundation of Hainan Province, China (No. 321RC465), and the Hainan University Mango Research System.

Conflict of interest

The authors declare that they have no conflict of interest.

Supplementary information accompanies this paper online at: https://doi.org/10.48130/tp-0026-0019.

Dates

Received 22 January 2026; Revised 27 April 2026; Accepted 6 May 2026; Published online 5 June 2026

References

[1] Janusz G, Pawlik A, Świderska-Burek U, Polak J, Sulej J, et al. 2020. Laccase properties, physiological functions, and evolution. *International Journal of Molecular Sciences* 21:966

[2] Dwivedi UN, Singh P, Pandey VP, Kumar A. 2011. Structure–function relationship among bacterial, fungal and plant laccases. *Journal of Molecular Catalysis B: Enzymatic* 68:117−128

[3] Hoffmann N, Benske A, Betz H, Schuetz M, Samuels AL. 2020. Laccases and peroxidases co-localize in lignified secondary cell walls throughout stem development. *Plant Physiology* 184:806−822

[4] Arregui L, Ayala M, Gómez-Gil X, Gutiérrez-Soto G, Hernández-Luna CE, et al. 2019. Laccases: structure, function, and potential application in water bioremediation. *Microbial Cell Factories* 18:200

[5] Upadhyay P, Shrivastava R, Agrawal PK. 2016. Bioprospecting and biotechnological applications of fungal laccase. *3 Biotech* 6:15

[6] Zhu C, Yin T, Chen Y, Wei S. 2025. Identifying and analyzing the laccase gene family in the genome of *Populus davidiana* × *P. bolleana*. *Molecular Plant Breeding* 1−14 (in Chinese)

[7] Barros J, Serk H, Granlund I, Pesquet E. 2015. The cell biology of lignification in higher plants. *Annals of Botany* 115:1053−1074

[8] Niu Z, Li G, Hu H, Lv J, Zheng Q, et al. 2021. A gene that underwent adaptive evolution, *LAC2* (LACCASE), in *Populus euphratica* improves drought tolerance by improving water transport capacity. *Horticulture Research* 8:88

[9] Qin S, Fan C, Li X, Li Y, Hu J, et al. 2020. *LACCASE14* is required for the deposition of guaiacyl lignin and affects cell wall digestibility in poplar. *Biotechnology for Biofuels* 13:197

[10] Berthet S, Demont-Caulet N, Pollet B, Bidzinski P, Cézard L, et al. 2011. Disruption of *LACCASE4* and *17* results in tissue-specific alterations to lignification of *Arabidopsis thaliana* stems. *The Plant Cell* 23:1124−1137

[11] Xu X, Zhou Y, Wang B, Ding L, Wang Y, et al. 2019. Genome-wide identification and characterization of laccase gene family in *Citrus sinensis*. *Gene* 689:114−123

[12] Cheng X, Li G, Ma C, Abdullah M, Zhang J, et al. 2019. Comprehensive genome-wide analysis of the pear (*Pyrus bretschneideri*) laccase gene (*PbLAC*) family and functional identification of *PbLAC1* involved in lignin biosynthesis. *PLoS One* 14:e0210892

[13] Balasubramanian VK, Rai KM, Thu SW, Hii MM, Mendu V. 2016. Genome-wide identification of multifunctional laccase gene family in cotton (*Gossypium spp.*); expression and biochemical analysis during fiber development. *Scientific Reports* 6:34309

[14] Ranocha P, Chabannes M, Chamayou S, Danoun S, Jauneau A, et al. 2002. Laccase down-regulation causes alterations in phenolic metabolism and cell wall structure in poplar. *Plant Physiology* 129:145−155

[15] Liu Q, Luo L, Wang X, Shen Z, Zheng L. 2017. Comprehensive analysis of rice laccase gene (*OsLAC*) family and ectopic expression of *OsLAC10* enhances tolerance to copper stress in *Arabidopsis*. *International Journal of Molecular Sciences* 18:209

[16] Turlapati PV, Kim KW, Davin LB, Lewis NG. 2011. The laccase multigene family in *Arabidopsis thaliana*: towards addressing the mystery of their gene function(s). *Planta* 233:439−470

[17] Zhao Q, Nakashima J, Chen F, Yin Y, Fu C, et al. 2013. *LACCASE* is necessary and nonredundant with *PEROXIDASE* for lignin polymerization during vascular development in *Arabidopsis*. *The Plant Cell* 25:3976−3987

[18] Wang CY, Zhang S, Yu Y, Luo YC, Liu Q, et al. 2014. *MiR397b* regulates both lignin content and seed number in *Arabidopsis* via modulating a

laccase involved in lignin biosynthesis. *Plant Biotechnology Journal* 12:1132−1142

[19] Le Bris P, Wang Y, Barbereau C, Antelme S, Cézard L, et al. 2019. Inactivation of *LACCASE8* and *LACCASE5* genes in *Brachypodium distachyon* leads to severe decrease in lignin content and high increase in saccharification yield without impacting plant integrity. *Biotechnology for Biofuels* 12:181

[20] Bryan AC, Jawdy S, Gunter L, Gjersing E, Sykes R, et al. 2016. Knockdown of a laccase in *Populus deltoides* confers altered cell wall chemistry and increased sugar release. *Plant Biotechnology Journal* 14:2010−2020

[21] Zhang Y, Wu L, Wang X, Chen B, Zhao J, et al. 2019. The cotton laccase gene *GhLAC15* enhances Verticillium wilt resistance via an increase in defence-induced lignification and lignin components in the cell walls of plants. *Molecular Plant Pathology* 20:309−322

[22] Xu X, Zhang Y, Liang M, Kong W, Liu J. 2022. The citrus laccase gene *CsLAC18* contributes to cold tolerance. *International Journal of Molecular Sciences* 23:14509

[23] Liu M, Dong H, Wang M, Liu Q. 2020. Evolutionary divergence of function and expression of laccase genes in plants. *Journal of Genetics* 99:23

[24] Zhang H, He H, Song W, Zheng L. 2023. Pre-harvest UVB irradiation enhances the phenolic and flavonoid content, and antioxidant activity of green- and red-leaf lettuce cultivars. *Horticulturae* 9:695

[25] Gupta SK, Sharma M, Deeba F, Pandey V. 2017. Plant response: UV-B avoidance mechanisms. In *UV-B Radiation: from Environmental Stressor to Regulator of Plant Growth*, eds. Singh VP, Singh S, Prasad SM, Parihar P. Chichester, UK: John Wiley & Sons Ltd. pp. 217−258 doi: 10.1002/9781119143611.ch12

[26] Gao Y, Wei L, Jiang C, Shi S, Jiao J, et al. 2025. Physiological mechanisms of the enhanced UV-B radiation triggering plant-specific peroxidase-mediated antioxidant defences. *Antioxidants* 14:957

[27] Rozema J, van de Staaij J, Björn LO, Caldwell M. 1997. UV-B as an environmental factor in plant life: stress and regulation. *Trends in Ecology & Evolution* 12:22−28

[28] Agati G, Azzarello E, Pollastri S, Tattini M. 2012. Flavonoids as antioxidants in plants: location and functional significance. *Plant Science* 196:67−76

[29] Hideg É, Jansen MAK, Strid Å. 2013. UV-B exposure, ROS, and stress: inseparable companions or loosely linked associates? *Trends in Plant Science* 18:107−115

[30] Sun Q, Zhou X, Yang L, Xu H, Zhou X. 2023. Integration of phosphoproteomics and transcriptome studies reveals ABA signaling pathways regulate UV-B tolerance in *Rhododendron chrysanthum* leaves. *Genes* 14:1153

[31] Müller R, Acosta-Motos JR, Großkinsky DK, Hernández JA, Lütken H, et al. 2019. UV-B exposure of black carrot (*Daucus carota* ssp. *sativus* var. *atrorubens*) plants promotes growth, accumulation of anthocyanin, and phenolic compounds. *Agronomy* 9:323

[32] Chen T, Peng J, Qian, M, Shui X, Du J, et al. 2023. The effects of enhanced ultraviolet-B radiation on leaf photosynthesis and submicroscopic structures in *Mangifera indica* L. cv. 'Tainong No 1'. *Horticulturae* 9:83

[33] Wang Q, Li G, Zheng K, Zhu X, Ma J, et al. 2019. The soybean laccase gene family: evolution and possible roles in plant defense and stem strength selection. *Genes* 10:701

[34] Tahir H, Sajjad M, Qian M, Ul Haq MZ, Tahir A, et al. 2024. Glutathione and ascorbic acid accumulation in mango pulp under enhanced UV-B based on transcriptome. *Antioxidants* 13:1429

[35] Birchler JA, Yang H. 2022. The multiple fates of gene duplications: deletion, hypofunctionalization, subfunctionalization, neofunctionalization, dosage balance constraints, and neutral variation. *The Plant Cell* 34:2466−2474

[36] Kong J, Xiong R, Qiu K, Lin X, Li D, et al. 2024. Genome-wide identification and characterization of the laccase gene family in *Fragaria vesca* and its potential roles in response to salt and drought stresses. *Plants* 13:3366

[37] Gong HL, Xing YJ, Ma JX, Cai X, Feng ZP. 2025. Identification of laccase (LAC) gene family in potato (*Solanum tuberosum* L.) and its expression analysis under salt stresses. *Biotechnology Bulletin* 41:82−93 (in Chinese)

[38] Panchy N, Lehti-Shiu M, Shiu SH. 2016. Evolution of gene duplication in plants. *Plant Physiology* 171:2294−2316

[39] Qiu KL, Wang YM, He JL, Yu H, Pan HF, et al. 2022. Identification of peach laccase family genes and functional analysis of *PpLAC21*. *Journal of Horticulture* 49:1351−1362 (in Chinese)

[40] Yang Y, Liu YY. 2021. Identification and sequence analysis of the *MdLAC* gene family members in apple. *Journal of Henan Agricultural Sciences* 50:125−135 (in Chinese)

[41] Yao W, Liu MM, Cheng MC, Liu SC. 2024. Genome-wide identification and expression analysis of LAC gene family of *Amaranthus tricolor* L. *China Vegetables* 11:48−56 (in Chinese)

[42] Waadt R, Seller CA, Hsu PK, Takahashi Y, Munemasa S, et al. 2022. Plant hormone regulation of abiotic stress responses. *Nature Reviews Molecular Cell Biology* 23:680−694